Article

Towards improved flash flood forecasting using WRF-Hydro in the horn of Africa: Case of Dire Dawa, Ethiopia

Addisu G. Semie [1,*], Gulilat T. Diro [2], Teferi Demissie [3], Yonas M. Yigezu [1] and Binyam Hailu [1]

[1] Addis Ababa University, Computational Data Science Program,city=Addis Ababa,postcode=1176
[2] ESCER Center, University of Quebec at Montreal, 201 President-Kennedy Avenue, H2X 3Y7, Canada , city=Montreal
[3] International Livestock Research Institute, city=Addis Ababa,postcode=5689
* Correspondence: addisu.semie@aau.edu.et

Abstract: A reliable flood early warning system must take into account the mechanisms that cause heavy precipitation events and accurate surface hydrology modeling. In this project, analysis of atmospheric processes and hydrological modelling of selected flood events over Dire Dawa is conducted using various observational/reanalysis data and uncoupled WRF-Hydro model simulations. To comprehend the processes causing such severe precipitation occurrences, large scale atmospheric fields linked to selected extreme precipitation events are examined using ERA5 reanalysis. The land surface was configured at 1 km resolution while 250 m sub-grid resolution was set to perform the routing process. Model forcing for the uncoupled WRF-Hydo model is obtained from ERA5 reanalysis data. Sensitivity of stream-flow simulation to various parameter values such as hydrolic conductivity and surface infiltration coefficient was carried out for August 2006. The result of the sensitivity experiment reveals that infiltration-runoff, hydrolic soil conductivity and saturated volumetric soil moisture with the parameter value of 0.1, 1.5 and 1.0, respectively are found to produce realistic spatial and temporal distribution of stream-flow. The extreme flood events of March 2005 and April 2007 were studied further to assess the performance of WRF-Hydro model and to understand the underlying atmospheric mechanisms causing these heavy precipitation events. The result of hydrological simulation demonstrated that uncoupled WRF-Hydro simulation reproduced both the temporal evolution and the spatial pattern reasonably well. Our analysis indicated that the amount of precipitation during these two events exceeded the long-term average by several factors, furthermore, the anomalies cover larger areas of eastern Ethiopia. Associated to these extreme events, upper level subtropical westerly jet-streams were anomalously stronger and also extended further southward favouring upper level divergence over the region. At lower level, the notable circulation anomalies include anomalous positive pressure anomaly over Sudan/Egypt leading to northerly flow anomaly over Red Sea, strengthening of southerly influx from southern Indian ocean due to stronger Mascarene High. The encouraging results from WRF-Hydro simulation suggest that this modelling framework can be implemented in operational context within national and regional forecasting centers as a key component to establish a flood monitoring and early warning system.

Keywords: WRF-Hydro; flood; extreme events; Ethiopia

Citation: Semie, A.G.; Diro, G.T. ; Demissie, T.; Yigezu, Y.M.; Hailu, B. Title. *Preprints* **2023**, *1*, 0. https://doi.org/

1. Introduction

The frequency and severity of floods in Africa have grown over the past several decades, which has had a substantial impact on the people and infrastructure of the continent [1]. For instance, in September 2009, 16 nations in West Africa were affected by torrential rain and flooding, which left 600,000 people in a difficult situation. This incident occurred shortly after the 2007 floods, which caused more than a million people to be displaced and claimed more than 500 deaths in nations including Uganda, Ethiopia, Sudan, Burkina Faso, Togo, Mali, and Niger, as well as the 2008 floods in Mozambique [2]. Floods in Africa frequently result in extensive damage to crops and loss of infrastructure, including roads, bridges, and buildings, which causes food shortages and famine. In addition, flooding in Africa worsens the spread of water-borne illnesses like cholera and

 doi:10.20944/preprints202305.0168.v1

typhoid, which has an even greater negative effect on community health and well-being [3].

Several episodes of extreme precipitation or lack of it have led to high-impact floods and droughts over East Africa. Furthermore, the frequency of the fatality caused by intense precipitation events and flash floods is increasing with time [4]. For instance, in the city of Dire Dawa, flash floods frequently resulted from significant rainfall events, which had disastrous effects on both infrastructure and occupants [5–7]. Spring is the season when the majority of heavy precipitation events occurs over Dire Dawa. The 2005 flood event that caused the death of more than 35 people and an estimated amount of 10 million birr damages to property due to the heavy precipitation and flood occurred in the spring season [8]. It is important to note that floods can also occur during summer season where it is the main rainy season for most of the western and central highland areas. For instance, in 2006 more than 200 people were dead and 3,000 displaced by flash floods that occurred in August [9]. In addition, coupled climate models broadly project an increase in the frequency of heavy precipitation over several parts of the world in the future warmer world due to an increase in anthropogenic greenhouse gas emission [10–14]. However, projections from global models are subject to uncertainty at regional and local city-scale due to their coarse resolution. This implies that there is a need for a realistic simulation and a thorough understanding of the flood characteristics in current climate in order to plan for a proper adaptation strategy.

Operational centers in East Africa, provide flood early warnings entirely based on precipitation outlooks with little emphasis on surface processes that play key role in modulating flood events. Numerous studies (for example, [15–18]) have demonstrated that high resolution land surface based hydrological models are able to simulate the pick, timing and spatial distribution of flood events reasonably. For instance, recent research by [16,19] indicated that the model capability for streamflow simulation after calibrating the uncoupled WRF-Hydro model in two basins (the Gila River and Babocomari River basins) in southern Arizona. Similar research by [20] demonstrated that WRF-Hydro modeling framework accurately reproduces flash flood behavior and can fairly predict runoff observations throughout six watersheds on New Caledonia's tropical island(SW Pacific). Furthermore, [21] employed WRF-Hydro model over the Tana river basin in East Africa to quantify the terrestrial water balance. However, less emphasis is given on the use of land surface based hydrological models for flood prediction over East Africa. Therefore, one of the objectives of this paper is to configure, simulate, calibrate and verify if the uncoupled WRF-hydro can be used to predict flood events.

Detailed investigation and understanding of meteorological and hydrological processes associated with these extreme precipitations that led to past flooding events can be of value to improve early warning systems. Past studies suggested the main large scale atmospheric factors causing heavy precipitation at sub-seasonal and seasonal time scale in the region are linked to the intensity of the high-pressure system over the Arabian sea, the southward shift of subtropical westerly jet streams, North Atlantic oscillation [22] and Madden-Julian Oscillation (MJO) [23]. Nonetheless, the corpus of scientific research on heavy rainfall events that cause floods in East Africa, particularly at short time scales in metropolitan areas, is still rather small. This paper is, therefore, aims to investigate the role of large scale atmospheric and oceanic features associated with recent high impact flooding events occurred in Dire Dawa. We will investigate the details of the synoptic evolution and infer the intensity of these events from climatological perspectives.

The paper is set up as follows. The data, method and model description are provided in Section 2. Section 3 will discuss the calibration of the uncopuled WRF-Hydro model. Main results of WRF-Hydro case studies together with meteorological analysis are discussed in Section 4. Finally summary and thoughts on future work are provided in Section 5.

Preprints (www.preprints.org) | NOT PEER-REVIEWED | Posted: 4 May 2023 doi:10.20944/preprints202305.0168.v1

2. Domain, Data and Model description

2.1. study area

The Eastern region of Ethiopia contains distinctive topographical features that can control regional hydrological phenomena. Figure 1a-b show several topographic features of interest, as well as providing the location of Dire Dawa city and its environs. Notable among the topographic features are the mountain ranges surrounding the city. These topographic characteristics have a significant impact on the development and organization of the hydrology linked to heavy precipitation.

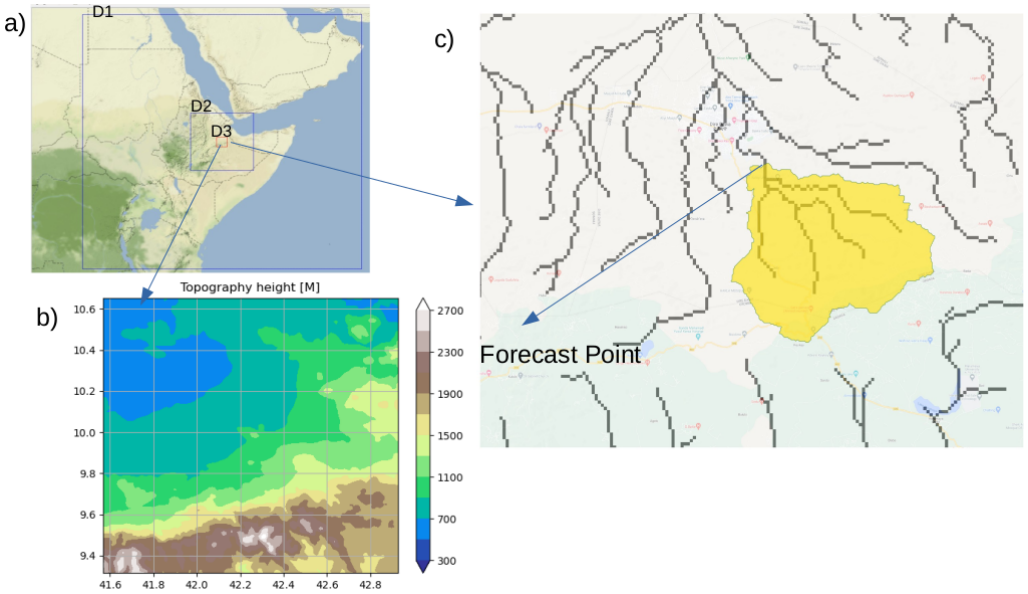

Figure 1. 1a) Map of East Africa showing the location of model domains at 25, 5 and 1-km horizontal resolution (D1, D2 and D3, respectively). D1 is defined by 150 × 150 grid points and extends 0 to 17 ^{0} N and 30 to 55^{0}E), D2 and D3 are defined with 150x150 grid points, b) Topography of D3 domain c) river channels in D3 domain with the focus of Dechatu river catchment (yellow shade) and forecast point.

This study is being carried out in the Ethiopian city of Dire Dawa, which frequently experiences flooding hazards. Here we are interested to investigate the Dechatu river catchment which is believed to be the cause of severe flash flooding in Dire Dawa city [5]. The Dechatu River pointed in the N-NW direction as indicated in figure 1c and it is originated in the northern escarpment of Harerge plateau.

Figure 2 indicates the maps of Land category and soil type in 1-km pixels of Dechatu river catchment derived from Moderate Resolution Imaging Spectroradiometer (MODIS) dataset. Grasslands and Open Shurblands are dominant land classes in this catchment as indicated in 2a. The whole dechatu river catchment indicated to have clay loam soil type as shown in figure 2b. Clay loam is a soil mixture that contains more clay than other types of rock or minerals. One of clay's most significant qualities is the size of its particles, which is quite small. As a result, loams that contain a predominance of clay tend to be heavy, because they are so dense.

Preprints (www.preprints.org) | NOT PEER-REVIEWED | Posted: 4 May 2023 doi:10.20944/preprints202305.0168.v1

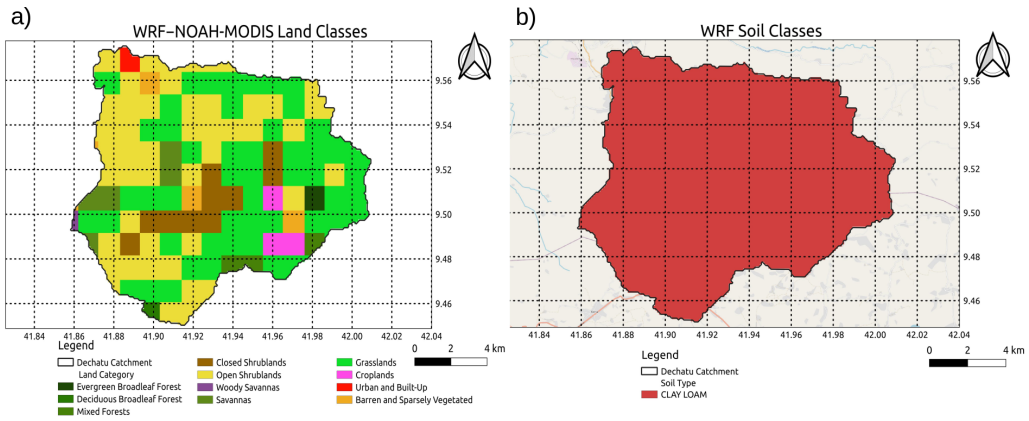

Figure 2. Maps of dominant a) Land category and b)soil type of Dachatu river catchment.

In gridded routing, the WRF-Hydro model's FLOWDIRECTION variable clearly describes flow directions along the channel network. This factor determines where water enters channels both from the surface of the ground and inside the channel. Figure 3a indicates the WRF-Hydro default flow direction grid along the Dechatu river catchment. We used the void filled digital elevation data of HydroSHEDS core products to validate the flow direction obtained from WRF-Hydro model. The flow direction acquired from HydroSHEDS data along Dechatu river catchment is indicated in figure 3b. The flow direction in the figure is similar to that of figure 3a, which means the flow direction attained from the WRF-Hydro model reasonably represent the flow direction along the Dechatu river catchment.

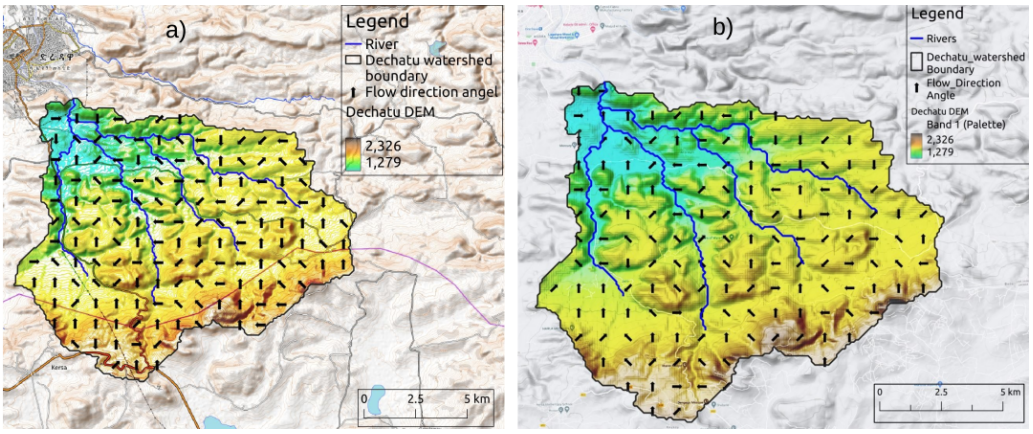

Figure 3. a) Dechatu river watershed along with WRF-Hydro default flow direction b) Dechatu river Watershed along with Hydroshed flow direction.

2.2. Observational and gridded datasets

We used several atmospheric variables (wind, radiation, temperature, humidity, surface pressure and precipitation) from ERA5 [24] reanalysis data and verification rainfall data from merged satellite-gage precipitation observations [25],[26]. The European Centre for Medium-range Weather Forecasts's (ECMWF) ERA5 is produced by assimilating observations and the Integrated Forecast System at a resolution of 0.25^{o} and available from 1979 until near-real-time [24].

The observed flow depth of Dechatu river catchment is provided with daily resolution from Ethiopian Ministry of Water and Energy. To conduct the comparison, we consider the daily maximum of the flow depth measured at the outlet of the Dechatu river obtained from the uncoupled WRF-Hydro model for the specified period.

Two daily observational precipitation datasets were used. These are the Global Precipitation Climatology Centre [26], which is available at 1 degree resolution for the 1988-2005

 doi:10.20944/preprints202305.0168.v1

period and precipitation dataset from the climate hazards infrared precipitation with station [25]. CHIRPS is built by combining station data with infrared satellite estimated precipitation, making it appealing for regions with a scarcity of data, like Africa. CHIRPS data is available from 1981 on wards. Both datasets are interpolated on to a common 0.25^0 grid resolution.

The 250m, 1km, and 5km spatial resolution Digital Elevation Model (DEM) data were generated by [27]. These DEMs were obtained from EarthEnv: Global, Remote Sensing Supported Environmental Layers for Assessing Status and Trends in Biodiversity, Ecosystems, and Climate http://www.earthenv.org/topography. The former, GMTED ([28]) served as the main data set due to its full global extent and having the highest resolution (250 m). In areas where the scopes of the two data sets overlap (56S–60N latitude), the later SRTM ([29]), created by the Consultative Group for International Agriculture Research - Consortium (CGIAR), was utilized for comparing and validating the GMTED-derived variables and evaluating the impact of spatial scale acquisition.

2.3. Model description

The uncoupled hydrological modeling system used in this study consists of the two models, the non-hydrostatic Weather Research and Forecasting (WRF) model [30] which is used to define the domains and initial conditions. The other model is WRF-Hydro which is responsible for handling the hydrological process. A brief overview of these two models is presented in section 2.3.1 and 2.3.2.

2.3.1. WRF model

WRF model version 4.3 [30] is employed in this paper. The model consists of three nested domains as indicated in Fig. 1a. The parent domain, D1 has 25-km horizontal resolution and it is defined with 150x150 grid points. The D1 domain is covering Sudan, South Sudan, Uganda, Kenya, Ethiopia, Eritrea, Somalia, Yemen and parts of Indian Ocean ($0^o$to 17^o N and 30^o to 55^o E), thus capturing a broad range of weather systems. D2 and D3 are defined with 150x150 grid points with horizontal resolution of 5-km and 1-km, respectively.

The D3 domain and the associated stream channels are indicated in Fig. 1c. The D3 domain further decomposed to finer horizontal resolution of 250m to handle the routing process. The simulation setup related to the routing processes will be explained further in section 2.3.2.

The simulations are initialized on January 1, 2006. NCEP (National Centers for Environmental Prediction) FNL(Final) operational global analysis data [31] provides the initial and lateral boundary conditions for the simulations. Further details of the WRF configurations and physics schemes and parameter setting used in this study are indicated in Table 1.

 doi:10.20944/preprints202305.0168.v1

Table 1. Configuration details of the atmospheric model, WRF

Namelist Parameter	Chosen option
Number of nested domains	3
Horizontal resolution	25km, 5km and 1km
Horizontal grid number	150x150 grids for D1, D2 and D3
Integration time-step	100s for D1
Projection resolution	Mercator
Vertical layers	34
Microphysics sheme	New Thompson et al. Scheme
Cumulus convection	Kain-Fritsch (KF) for D1, no convection scheme for D2 and D3
Planetary boundary layer	Yonsei University Scheme
Longwave radiation	RRTMG
Shortwave radiation	RRTMG
Land Surface Sheme	5–layer Thermal Diffusion Scheme
Land use	Modis
Surface layer	Revised MM5 Scheme

2.3.2. WRF-Hydro model

The WRF-Hydro model is a distributed, community-based system that integrates the WRF atmospheric model with simulation modules for lateral water flow and aquifer activities [32]. Both uncoupled (independently or offline) and coupled (in combination with other Earth System modeling systems, such as an atmospheric model) applications of the model are possible. This study used the uncoupled WRF-Hydro model to investigate flooding events in Dire Dawa.

The uncoupled mode functions like any other land surface hydrological modeling system and behaves as a standalone Land Surface Model (in our instance, Noah-MP LSM). It needs gridded meteorological forcing data that has been prepared and provided externally. Major land surface processes such as surface energy balance, runoff production and infiltration, aquifer recharge, and snow melt and accumulation are handled by Noah-MP LSM. Runoff generation and infiltration processes are discussed further in section 2.4, since we noticed the parameters related to this process are critical for model calibration for our study area. Table 2 lists the physics options used for the application of Noah-MP.

Preprints (www.preprints.org) | NOT PEER-REVIEWED | Posted: 4 May 2023 doi:10.20944/preprints202305.0168.v1

Table 2. Selected physics options of Noah-MP LSM. The ID numbers are used to identify the values that can be entered into the model input file.

Processes	Option ID in WRF-Hydro	Description
DYNAMIC_VEG_OPTION	4	Using monthly LAI is prescribed for various vegetation types
CANOPY_STOMATAL_RESISTANCE OPTION	1	Ball-Berry – Canopy stomatal resistance
BTR_OPTION	1	Noah type using soil moisture for stomatal resistance
RUNOFF_OPTION	3	Noah type surface and subsurface runoff (free drainage)
SURFACE_DRAG_OPTION	1	Monin-Obukhov
FROZEN_SOIL_OPTION	1	Using the total soil moisture to compute hydraulic properties
SUPERCOOLED_WATER_OPTION	1	No iteration (Form of the freezing-point depression equation)
RADIATIVE_TRANSFER_OPTION	3	Two-stream applied to vegetated fraction
SNOW_ALBEDO_OPTION	2	BATS
PCP_PARTITION_OPTION	1	Jordan (1991)
TBOT_OPTION	2	TBOT at ZBOT (8m) read from a file
TEMP_TIME_SCHEME_OPTION	3	Semi-implicit; flux top boundary condition, but FSNO for TS calculation
GLACIER_OPTION	2	Ice treatment more like original Noah
SURFACE_RESISTANCE_OPTION	4	For non-snow; rsurf = rsurf_snow for snow (set in MPTABLE)

2.4. Runoff generation and infiltration

Four soil layers that extends up to 2 meters are used: 0.1 m, 0.3 m, 0.6 m and 1 m thickness for 1^{st}, 2^{nd}, 3^{rd} and 4^{th} layers, respectively. Depending on the moisture content of the soil and the amount of precipitation, runoff can be created or water can infiltrate through the soil layers and percolate to an underlying unconfined aquifer. In this work, runoff production was simulated using the infiltration-excess-based surface runoff schemes ([33] and [34]).

Surface runoff, R, equals the difference between precipitation, P, and maximum infiltration, I_{max} ($R = P - I_{max}$). Infiltration maximum I_{max} is computed as an increasing function of the liquid soil moisture deficit of the soil column D_{total}:

$$I_{max} = P_x.\{\frac{D_{total}[1 - exp^{(\frac{DKSAT.REFKDT.\Delta t_1}{REFDK})}]}{P_x + D_{total}[1 - exp^{(\frac{DKSAT.REFKDT.\Delta t_1}{REFDK})}]}\} \quad (1)$$

Where Δt_1 is time step of the model, depending on soil texture, REFDK is a reference saturated hydraulic conductivity of silty clay loam, assumed spatially constant and equal to $2x10^{-6}m/s$, DKSAT is the saturated hydraulic soil conductivity, and REFKDT is the surface infiltration coefficient. The value of REFDK and REFKDT are constant on the whole domain.

2.5. Model Performance Evaluation metrics

Some quantitative data is needed to measure model performance in order to calibrate, validate, and compare the models. The flow depth data collected at the Dechatu river

Preprints (www.preprints.org) | NOT PEER-REVIEWED | Posted: 4 May 2023 doi:10.20944/preprints202305.0168.v1

watershed's outlet is used in this study to evaluate the model's performance. We used statistical indices such as such as the Nash-Sutcliffe efficiency (NSE), Root Mean Square Error (RMSE) and RMSE observations standard deviation ratio (RSR) to quantify model performance.

The range of the Nash-Sutcliffe efficiency coefficient (NSE) is -∞ to 1. When NSE = 1 (Equation A3), it denotes a perfect agreement between the observed and anticipated values. In general, values between 0.0 and 1.0 are regarded as acceptable performance levels [35], but values below 0.0 show that the mean observed value is higher than the simulated value, which denotes unacceptable performance. When the RMSE (Equation A4) equals 0, the observed and predicted values match perfectly, and as the RMSE increases, the quality of the simulation deteriorates. The ratio of the RMSE and standard deviation of measured data is used to determine the RMSE-observations standard deviation ratio (RSR) as shown in Equation A5. RSR ranges from a high positive value to the ideal value of zero. The performance of the model simulation increases with decreasing RMSE, and RSR.

3. Results and Discussion

3.1. Calibration of the uncopuled WRF-Hydro model

Many parameters in the uncoupled WRF-Hydro model have significant uncertainty that can potentially alter the calculation of the runoff as indicated in equation 1 to A2.

A 2-months spin up simulations was performed prior to the calibration to ensure the numerical stability of the model outputs. We used default configuration with the original surface and subsurface runoff option ($RUNOFF\_OPTION = 3$). The default configuration parameters have values of 3.0, 1.0 and 1.0 for REFKDT, DKSAT and SMCMAX, respectively. Meteorological forcing data extracted from ERA5 dataset. The standalone WRF-Hydro model requires eight meteorological input variables that includes: hourly Incoming shortwave radiation (SWDOWN), Incoming longwave radiation (LWDOWN), Specific humidity (Q2D), Air temperature at 2 meters above the surface (T2D), Surface pressure (PSFC), Near surface wind in the u-component (U2D), Near surface wind in the v-component (V2D) and Precipitation rate (RAINRATE). After the spin-up, "restart" NetCDF files were created and used to start the simulations on 1 August 2006 with the proper values for the state variables. The simulated stream discharge doesn't respond to the precipitation rate during the Model spin-up period (June 1 - July 31, 2006), shown in the supplementary Figure A1, and it continuously decrease throughout the simulation period. This means the model isn't doing a good job in representing the stream discharge.

To improve the results obtained during the Model spin-up, calibration is conducted on the parameters that control surface runoff. In this study, three parameters are taken into consideration for calibration: the surface runoff parameter (REFKDT), saturated hydraulic soil conductivity (DKSAT) and saturated volumetric soil moisture content (SMCMAX). These parameters are indicated in equations A1 and they have a potential to significantly affect the surface runoff. For instance, lower values of REFKDT and DKSAT result in a reduction in the soil column's ability to absorb water which minimize infiltration and in turn raises surface runoff (equation A1).

The simulated flow depth from the uncoupled WRF-Hydro model for the period of August 1 - 15, 2006 is compared to the observed flow depth at the Dechatu river catchment. This specific period is chosen as it had known for the occurrence of one of the largest and the most devastating flash flood in the city of Dire Dawa on August 6, 2006 [5]. We used a step-wise approach to reduce the number of model runs and wasteful computation time as recommended by [36].

The hydrograph volume is controlled by the REFKDT, whose feasible range is 0.1 to 10, with a default value of 3.0. In this paper, we looked at the range of 0.1 to 3.0 as indicated in Table 3. DKSAT has multiplicative factors that vary from 0.3 to 2 and is spatially variable. Similar to REFKDT, the DKSAT's default value of 1 serves the same purpose. During calibration, we consider the range 0.3 to 2.0 Table 3. Similar to DKSAT, SMCMAX vary spatially with multiplicative factors that ranges from 0.75 to 1.5 as shown in Table

 doi:10.20944/preprints202305.0168.v1

3. SMCMAX regulates the amount of water that can be held in the soil, which enables it to manage the soil's capacity for infiltration and the runoff that is produced, as shown in equations A1 and A2.

Table 3. Selective objective criteria (Nash-Sutcliffe efficiency (NSE) and the RMSE observation standard deviation ratio (RSR)) between simulated and observed discharges at Dechatu river catchment based on selected parameters infiltration-runoff (REFKDT), hydraulic soil conductivity (DKSAT), and saturated volumetric soil moisture (SMCMAX)

REFKDT						
Vaules	0.1	0.3	0.5	1	2	3
NSE	0.324	0.259	0.138	-0.01	-0.085	-0.086
RMSE	0.346	0.363	0.391	0.424	0.439	0.439
RSE	0.822	0.861	0.928	1.005	1.042	1.042
DKSAT						
Values	0.3	0.5	0.7	1	1.5	2
NSE	0.051	0.214	0.286	0.324	0.335	0.32
RMSE	0.41	0.374	0.356	0.346	0.344	0.347
RSE	0.974	0.887	0.845	0.822	0.816	0.825
SMCMAX						
Values	0.75	0.9	1	1.2	1.5	
NSE	0.317	0.333	0.335	0.325	0.297	
RMSE	0.348	0.344	0.344	0.346	0.353	
RSE	0.826	0.817	0.816	0.822	0.838	

Based on the selected objective criteria, namely the Nash-Sutcliffe efficiency (NSE) and the RMSE observation standard deviation ratio (RSR), the calibration results between the simulated and observed flow depth at daily resolution for the period of 15 days are presented in 3. Initially, the REFKDT parameter is considered to conduct the sensitivity experiments. When the REFKDT parameter is set to 0.1, the agreement between the simulated and observed flow depth at the Dechatu River catchment's exit shows the greatest value. Similarly, for this experiment the RMSE and RSR values are relatively smaller as indicated in Table 3. That means, the best value obtained for REFKDT calibration is 0.1. This value is fixed for the calibration of DKSAT and we found the simulation with DKSAT value of 1.5 to have a better model configuration. Similarly, we considered REFKDT = 0.1 and DKSAT = 1.5 to calibrate the SMCMAX. As displayed in Table 3, the optimum value SMCMAX is found to be 1.0.

Figure 4 displays the spatial pattern of the the stream discharge of the Dechatu river catchment with the associated tributaries. The intensity of the stream discharge is relatively lower in the tributaries and have maximum value at the forecast point. Based on the simulation with the calibrated parameters the highest stream discharge is observed on August 06, 2006 at 13hr, the river flow discharge also displays the highest intensity at this time (Figure 4a). Since the heavy rain didn't stay for longer period, the intensity of the stream discharge is lower in the next hour as indicated in figure 4b.

Preprints (www.preprints.org) | NOT PEER-REVIEWED | Posted: 4 May 2023 doi:10.20944/preprints202305.0168.v1

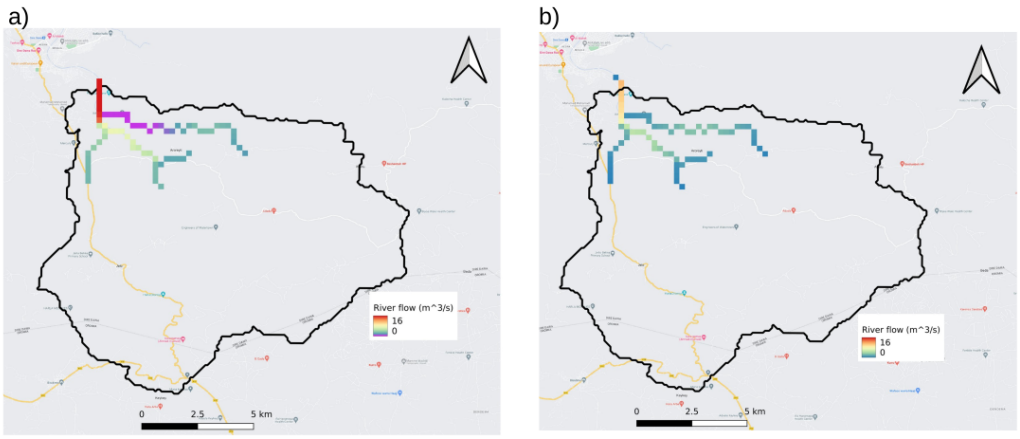

Figure 4. River flow that contributes to the Dechatu river at the forecast point a) August 06, 2006 at 13hr b) August 06, 2006 at 14hr.

The hourly simulated stream discharge at the Dechatu river with default and selected best parameters are compared in figure 5a. The simulation with the default parameters found to be non-responsive to the available precipitation in the domain. The stream discharge is almost zero throughout the simulation period on the other hand the simulation with calibrated parameters displayed to have higher volume of discharge immediately after largest precipitation is observed in the domain (figure 5a).

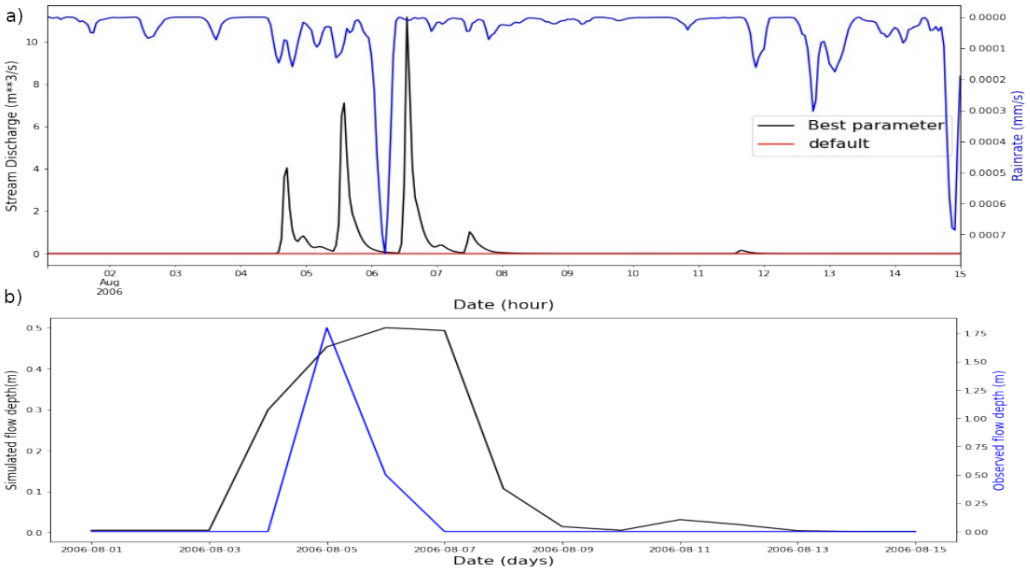

Figure 5. a) WRF-Hydro hourly stream discharge of default and calibrated parameters compared with the rainrate obtained from ERA5 data for the period of August 1 - 15, 2006 b) Daily simulated flow depth is compared with observed flow depth for the duration of August 1 - 15, 2006.

Figure 5b compares the daily observed and simulated flow depth (the simulation uses the calibrated parameters). The maximum flow depth of both the simulated and observed happens to occur on the similar date. This means, the simulated flow depth managed to identify the occurrence of the flash flood. However, the simulation underestimate the depth of the flash flood compared with the observed flow depth. It is critical to note that, unlike dynamical variables, the precipitation field in ERA5 reanalysis is greatly influenced by the physical parametrization in ECMWF model and hence related to the quality of short-range numerical weather prediction output. Comparison (not shown) indicated that ERA5 precipitation amounts are lower than that of WRFDEI (a bias adjusted precipitation

Preprints (www.preprints.org) | NOT PEER-REVIEWED | Posted: 4 May 2023 doi:10.20944/preprints202305.0168.v1

data generated using the same methodology as the widely used WATCH Forcing Data (WFD))over the study region highlighting the importance of accurate precipitation forcing.

Having observed the enhanced performance of WRF-hydro resulting from the modification of parameter settings described above, we proceeded to employ the calibrated model to investigate two recent extreme cases, which occurred in March 2005 and April 2007. The subsequent subsections will present a comprehensive analysis of the meteorological precursors, as well as a detailed account of the WRF-hydro simulation results.

3.2. Case study I (March 2005)

3.2.1. Extreme precipitation event and its association with circulation anomalies

The anomalous heavy precipitation event of March 2005 has affected most of the eastern and central Ethiopia but its most devastating impact was over Dire Dawa city. Figure 6 shows the spatial distribution of precipitation amount for the March 17-21, 2005 and its deviation from the corresponding long term average. It is clear that the precipitation amount in 2005 is much higher than the corresponding climatological values for most regions including over Dire Dawa.

This extreme precipitation event was associated with notable anomalies in oceanic and atmospheric circulation features. Although ENSO condition was not strong, the sea surface temperature anomaly (SSTa) distribution during the heavy rainfall event is characterized by a dipole pattern of sea surface temperature anomaly over southwestern Indian Ocean (Figure 7a). The dipole pattern is composed of a warm SST anomaly north of Madagascar and a cold sst anomaly over Mascarene. It is interesting to note that this dipole pattern of SST is co-located with a dipole pattern of sea level pressure anomaly, with stronger than normal Mascarene high and negative SLP anomaly over north of Madagascare as shown in Figure 7c. Such intensification of high pressure system over Mascarene is in line with strengthening of southerly influx of moisture from Indian ocean to eastern Africa as shown in Figure 8a. It is also important to note the unusual extended high pressure anomaly centered over Mediterranean sea (which is higher than the Azores high) but its extent reaches over northeast Africa and Middle-east. These causes northeasterly anomaly from north Africa, , easterly anomaly over northern Indian ocean converge with the southeasterly anomaly from southern Indian ocean as shown in the low level circulation anomaly (Figure 8 a and b). Upper level circulation features (Figure 8) revealed that the sub-tropical westerly Jetstream is intensified and shifted southward over north Africa during this extreme precipitation events. This upper level anomalous circulation is conducive to create upper level divergence. These upper and lower level circulation anomalies are inline with those reported in [22].

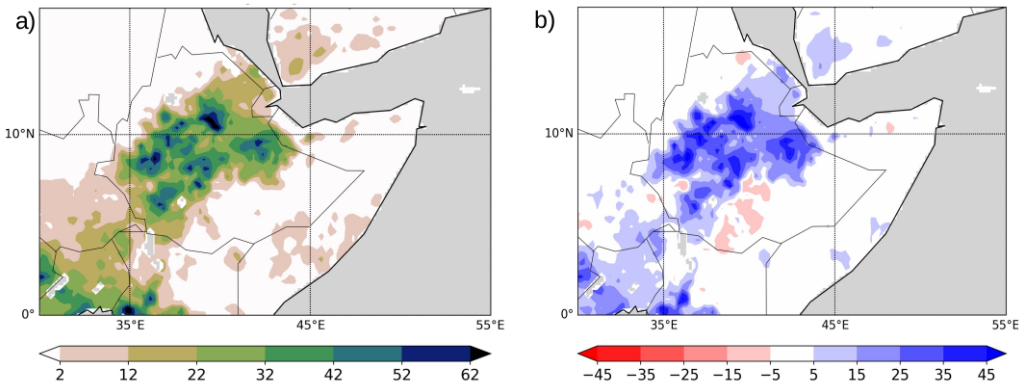

Figure 6. a) CHIRPS precipitation (mm) March [17 - 20, 2005] b) CHIRPS precipitation anomaly March [17 - 20], 2005 - Climatology [1991-2020].

Preprints (www.preprints.org) | NOT PEER-REVIEWED | Posted: 4 May 2023 doi:10.20944/preprints202305.0168.v1

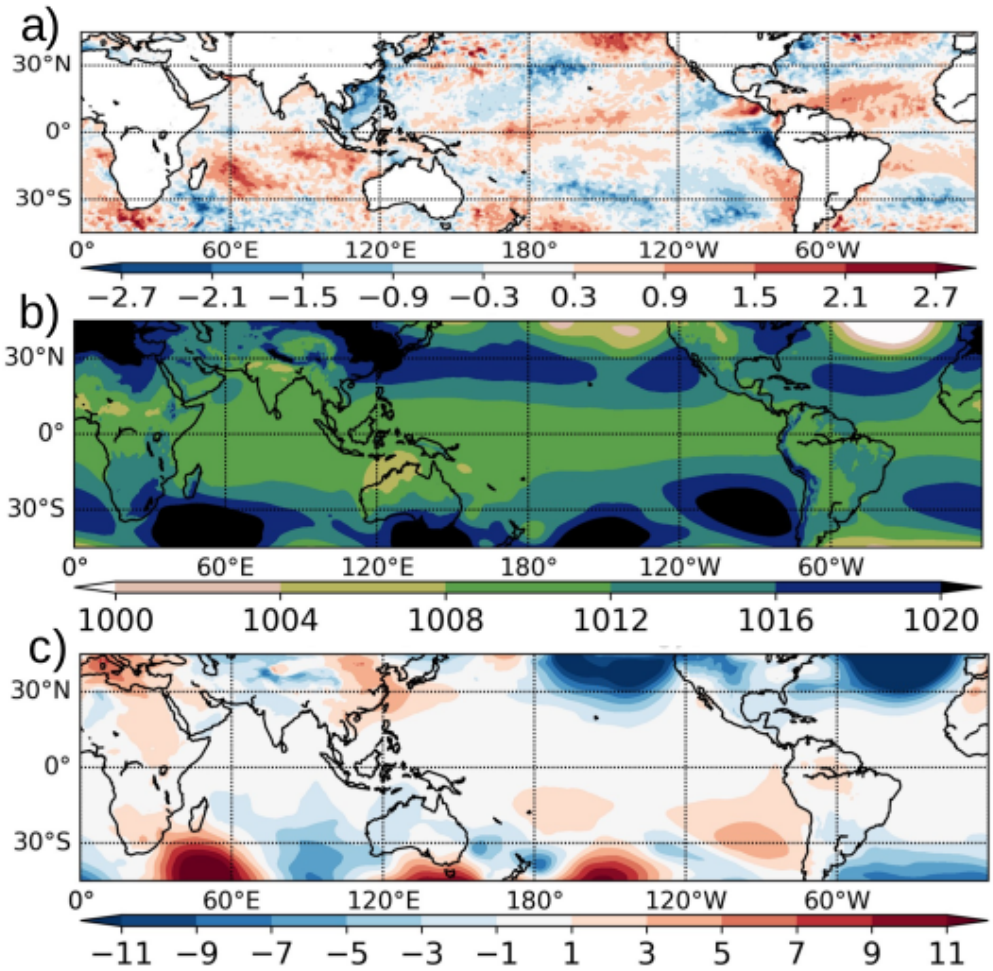

Figure 7. a) OI SST anomaly [oC] , March [17-21] 2005 - climatology [1991-2020] b) ERA5 SLP [hPa] March [17-21] 2005 c) ERA5 SLP anomaly [hPa] March [17-21] 2005 - climatology [1991-2020].

Preprints (www.preprints.org) | NOT PEER-REVIEWED | Posted: 4 May 2023 doi:10.20944/preprints202305.0168.v1

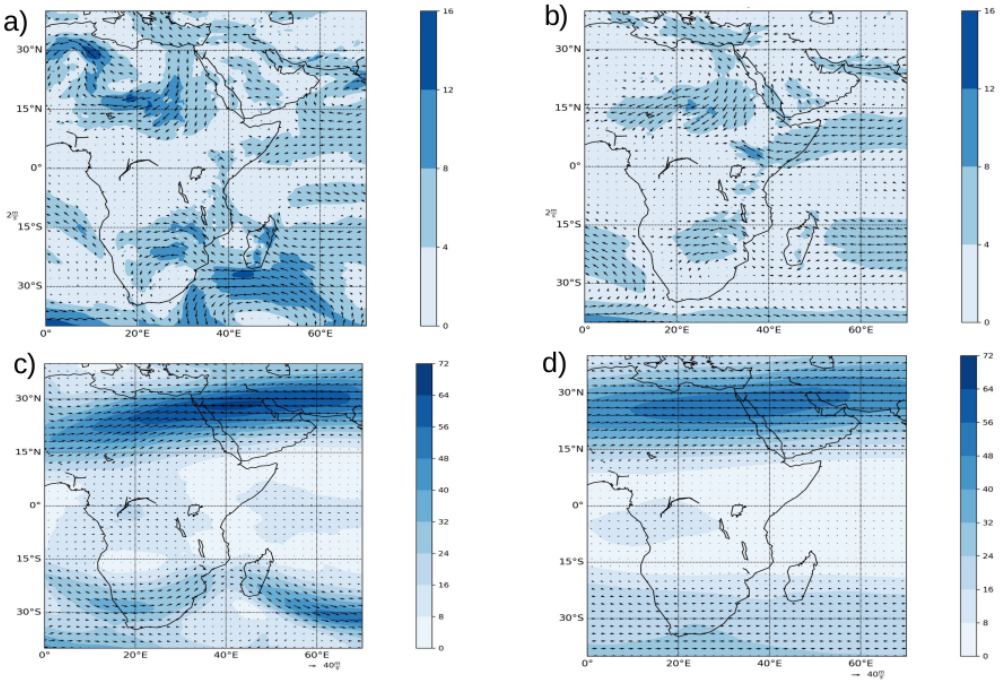

Figure 8. a) wind at 850hPa [ms^{-1}] for March 17-21 b) wind at 850hPa [ms^{-1}] for March 17-21 2005 - [1991-2020] climatology c) wind at 200hPa [ms^{-1}] for March 17-21, 2005 d) wind at 200hPa [ms^{-1}] for March 17-21, 2005 - [1991-2020] climatology.

3.2.2. WRF-hydro simulation for the case study of March 2005

The calibrated WRF-Hydro model is configured to investigate two well known flood events in Dire Dawa region. The first case study considers one of the flood events that occurred on March 20, 2005 [5].

Figure 9 a - h indicate the spatial distribution of the forcing precipitation field in the inner domain where higher resolution (1-km) hydrological model is conducted. Based on the forcing field, the precipitation that triggered the flood began on March 17, with a precipitation amount of 0.003-0.004 mm/s in the western part of the domain (Figure 9 b). Subsequently, on March 18, there was a widespread precipitation across the entire domain, with a precipitation amount of 0.006 mm/s in the highland region (Figure 9 c). On March 19th, there was further intense precipitation on the western edge of the domain, but a substantial amount of precipitation still fell over the highland area (Figure 9 d) . The highland regions received a significant amount of rainfall over the next two days, i.e., March 20 and 21, before the precipitation finally ceased (Figure 9 e - h).

Preprints (www.preprints.org) | NOT PEER-REVIEWED | Posted: 4 May 2023 doi:10.20944/preprints202305.0168.v1

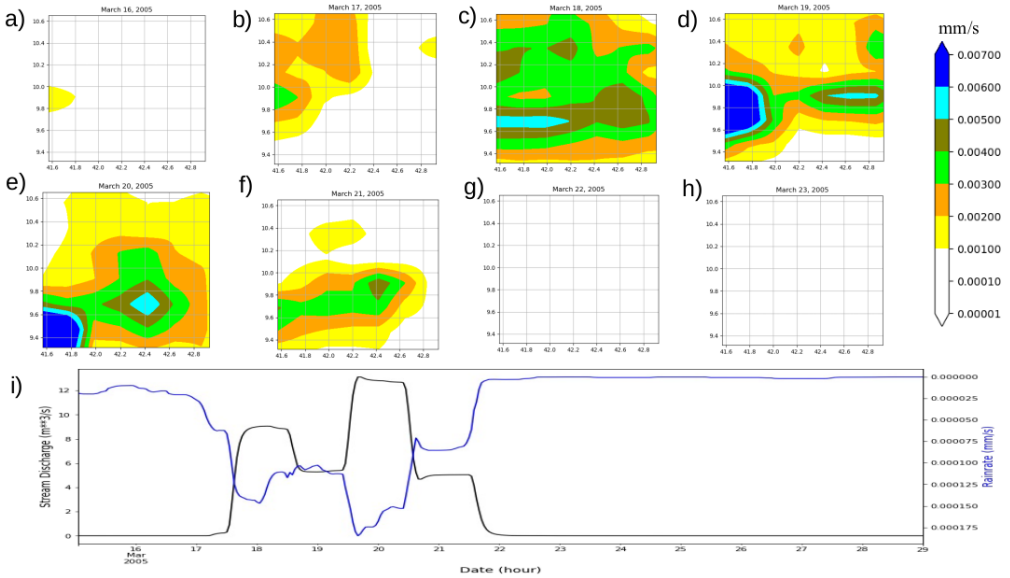

Figure 9. Spatial distribution of daily cumulative precipitation obtained from ERA5 reanalysis precipitation data for duration of March 15 to March 30, 2005, a - h, respectively. I) Time series with running mean of 24 hours of stream discharge (black) and rain rate (blue) for the period of March 15 - March 30, 2005.

In Figure 9 i, we calculated the average precipitation solely for the highland region. The simulated stream discharge began to rise on March 17, 2005, in response to the corresponding increase in input precipitation forcing. The peak stream discharge at the forecast point coincided with the highest mean precipitation in the domain, as depicted in Figure 9 i. In this instance, the simulation successfully replicated the flood event of March 20, 2005.

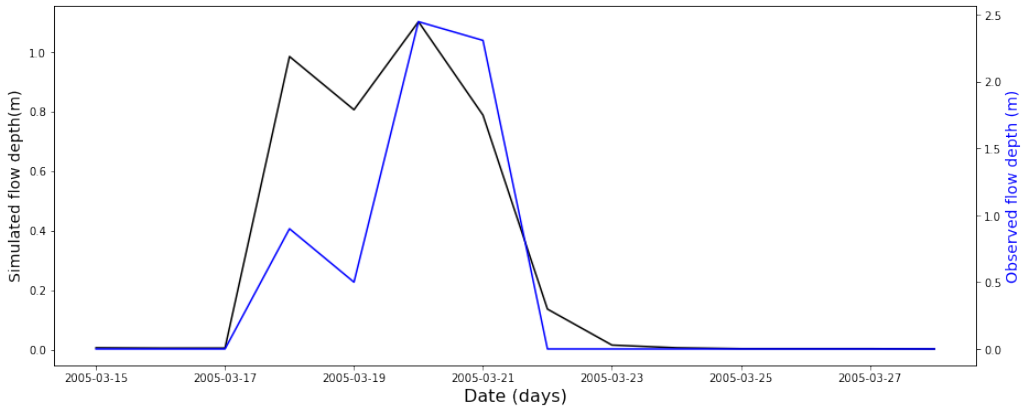

Figure 10. Daily simulated flow depth is compared with observed flow depth for the duration of March 15 - March 29, 2005.

The comparison of the observed and simulated maximum flow depths showed that the flash flood that occurred on March 20, 2005 was precisely detected by the simulated maximum flow depth (Figure 10) Subsequently, after the flood event, the flow depths of both the simulated and observed data decreased rapidly. However, compared to the measured flow depth, the simulation underestimated the depth of the flash flood; it should be noted that this was also the case during the flood of August 2006. The NSE value determined for this time period is discovered to be 0.56, which is within the hydrological analysis's acceptable range [35].

 doi:10.20944/preprints202305.0168.v1

3.3. Case study II (April 2007)

3.3.1. Climatological perspectives for the case of April 2007

During 12-16th April 2007, heavy precipitation events occurred over Easter Ethiopia (Figure 11). The precipitation amount exceeds the climatological values by over 20mm/day. Most of the heavy precipitation event occur over Dire Dawa leading to flash flood and high level of Dechatu river with dramatic consequence on people and infrastructure. One of the aim of this section is to identify the circulation type associated with the flood events.

The notable SST anomalies during April 2007 flood event include negative anomalies over Nino 1+2 region and warming anomalies over northwest Indian ocean (Figure 12). The sea-level pressure anomalies include weakening of the high pressure system over Arabian sea. However, positive anomalies are noted over Mascarene and over northeastern Sudan and Egypt regions. These patterns of positive sea level pressure anomalous are inline with the northerly flow anomalies over Red Sea and southerly flow anomalies from south Indian ocean which suggest an intensification of moisture influx to the Eastern and southern Ethiopia. At upper level, similar to the March 2005 case, the tropical westerly jet is shifted southward and also strengthened compared to climatological values which favors an upper level divergence.

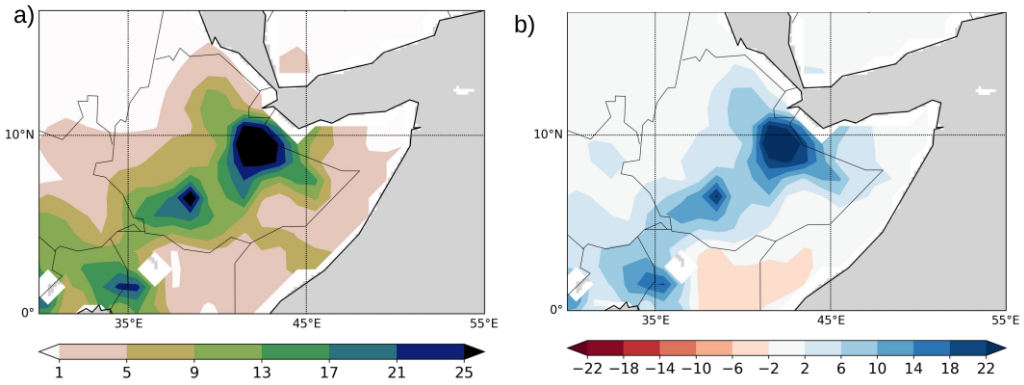

Figure 11. a) CHIRPS precipitation (mm) April [12 - 16, 2007] b) CHIRPS precipitation anomaly April [12 - 16], 2007 - Climatology [1991-2020].

 doi:10.20944/preprints202305.0168.v1

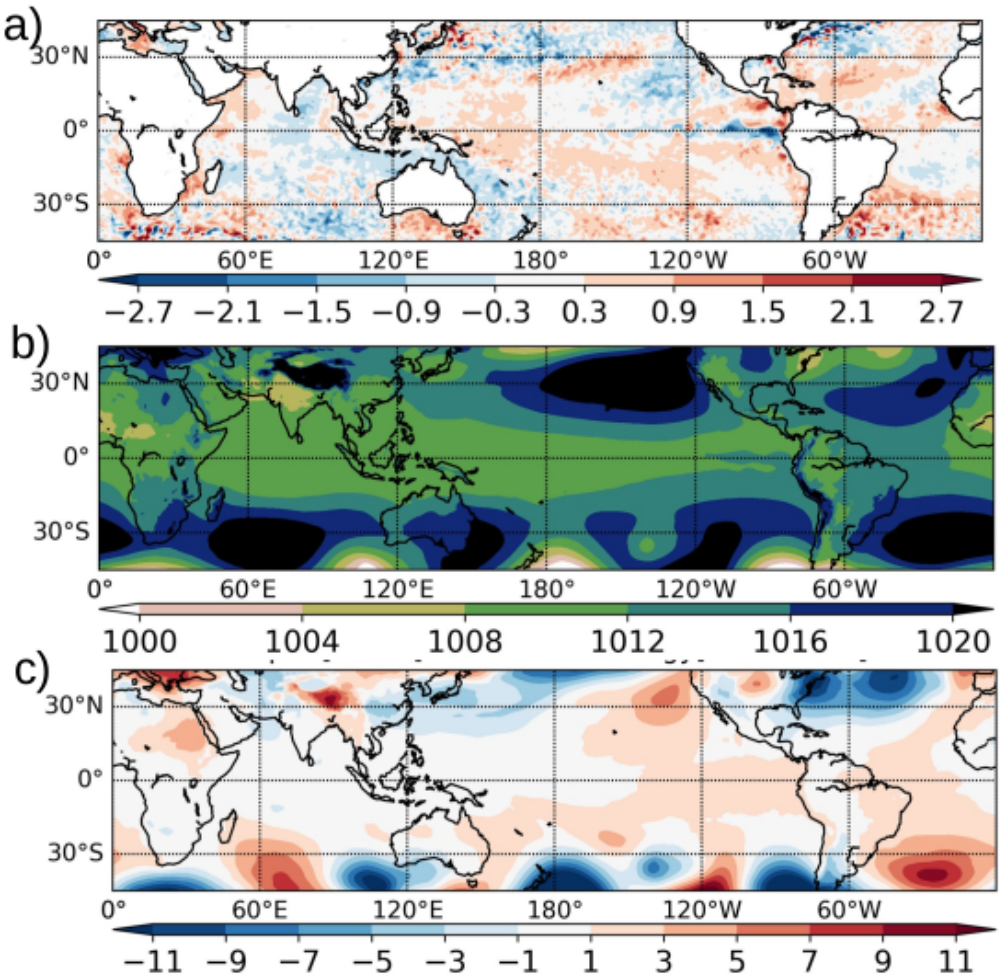

Figure 12. a) OI SST anomaly [oC] , April [12-16] 2007 - climatology [1991-2020] b) ERA5 SLP [hPa] April [12-16] 2007 c) ERA5 SLP anomaly [hPa] April [12-16] 2007 - climatology [1991-2020].

Preprints (www.preprints.org) | NOT PEER-REVIEWED | Posted: 4 May 2023 doi:10.20944/preprints202305.0168.v1

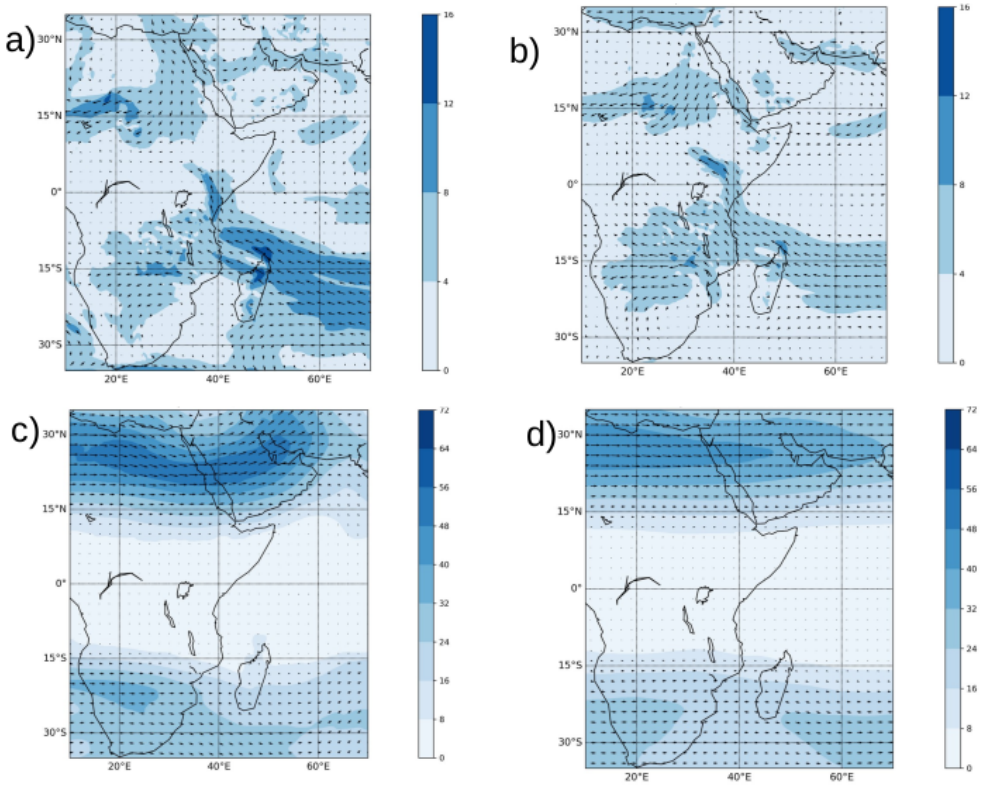

Figure 13. a) wind at 850hPa [ms^{-1}] for April 12-16 b) wind at 850hPa [ms^{-1}] for April 12-16 2007 - [1991-2020] climatology c) wind at 200hPa [ms^{-1}] for April 12-16, 2007 d) wind at 200hPa [ms^{-1}] for April 12-16, 2007 - [1991-2020] climatology.

3.3.2. WRF-hydro simulation for the case study of April 2007

The other flood event that is considered in this case study happened on April 12, 2007 [5]. The spatial distribution of precipitation in the inner domain displays a relatively less precipitation (less than 0.006 mm/s) on the specified date as shown in Figure 14c. Following that, a widespread precipitation occurred across the entire domain on April 13, 2007, with a precipitation amount of 0.006 mm/s in the highland region (Figure 14 d). On April 14th, there was further intense precipitation throughout the domain (Figure 14 e). The highland regions experienced significant rainfall for the next two days, i.e., April 15 and 16, before the precipitation eventually stopped (Figure 14 f-h).

Preprints (www.preprints.org) | NOT PEER-REVIEWED | Posted: 4 May 2023 doi:10.20944/preprints202305.0168.v1

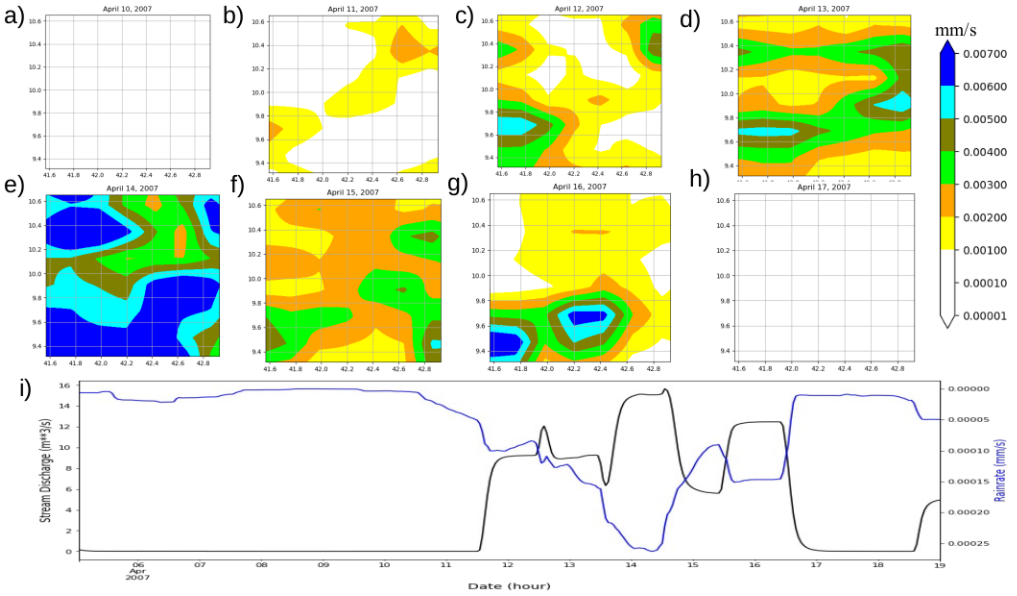

Figure 14. Spatial distribution of daily cumulative precipitation obtained from ERA5 reanalysis precipitation data for duration of April 5 to March 19, 2007, a - h, respectively. I) Time series with running mean of 24 hours of stream discharge (black) and rain rate (blue) for the period of April 5 - April 19, 2007.

Figure 14i indicate an increase in the flow discharge at the Dechatu river forecast point on April 12, 2007. In this case the model seems to detect the signature of the flood event even if the signal from the input data isn't that strong. Unlike our first case study, the representation of the flood event isn't exactly on the same day as that of the historical recorded flood event [5]. The WRF-Hydro indicates the highest stream discharge on April 14, 2007, that means it is off by two days when it compared to the historical data. The input precipitation ERA5 data (Figure 14e) might play a critical role in delaying the representation of the flood event in the Hydrological model.

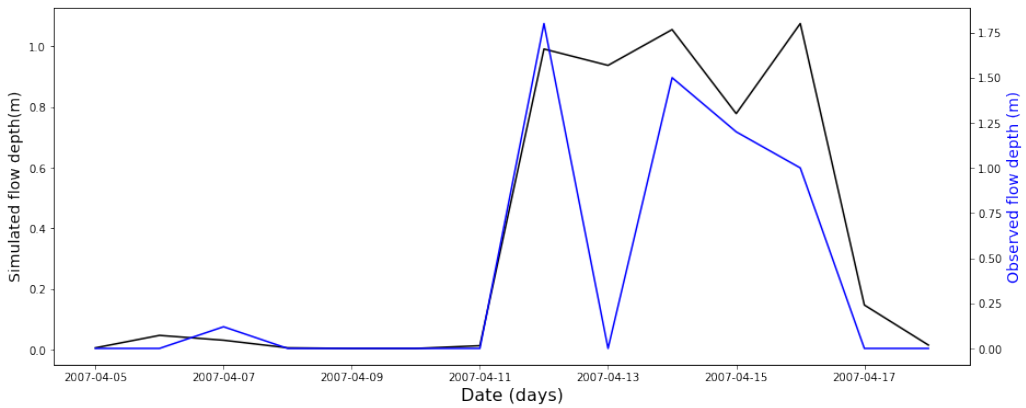

Figure 15. Daily simulated flow depth is compared with observed flow depth for the duration of a) March 15 - March 29, 2005 b) April 5 - April 18, 2007.

The model was able to replicate the timing of the flood event by accurately simulating the onset and cessation of the flood event. Specifically, the simulated maximum flow depth started increasing on the same day as the observed data and decreased on a similar day as the observed data. However, the simulation results indicated a discrepancy in the detection of the flash flood that took place on April 12, 2007. The Figure 15 revealed a two-day gap between the peak of the observed and simulated flow depth. As in the previous case study, the simulation underestimated the depth of the flash flood, which may be attributed to the

 doi:10.20944/preprints202305.0168.v1

ERA5 input data. Nevertheless, the NSE value calculated for this period is 0.66, which falls within the acceptable range of the hydrological analysis [35].

4. Summary and Conclusions

In terms of both human impacts and economic losses, flooding stands out as one of the most significant types of natural disasters [37,38]. In many parts of Africa, floods have caused damage to crops, loss of infrastructure and worsens the spread of water-borne diseases. Furthermore, the frequency and intensity of flood events have increased in recent decades [1].

Therefore, it is crucial to develop a modeling capability and understanding of flood events for early warning systems. With this goal in mind, a WRF-Hydro model has been configured at a 1km (250m) resolution over the Horn of Africa to simulate major flood events in the Eastern Ethiopia domain.

Multiple sensitivity experiments have been performed with WRF-hydro model to comprehend and portray the impact of different parameter values on streamflow response. These experiments were conducted for August 2006 events and the most sensitive parameters are found to be hydraulic conductivity, surface infiltration coefficient and saturated volumetric soil moisture. The result of these experiments aided in obtaining suitable parameter values of 0.1 for infiltration-runoff, 1.5 for hydraulic soil conductivity, and 1.0 for saturated volumetric soil moisture. Using the adjusted parameters in the experiments, the model is able to accurately represent the crucial aspects of the flood event, such as the start, peak, and end timings.

To evaluate the performance of the configured WRF-hydro model, we conducted tests using data from two flood episodes that occurred in March 2005 and April 2007. The results revealed NSE values of 0.56 for March 2005 and 0.66 for April 2007 flood events. In addition the WRF-hydro model demonstrated it's ability to capture the timing and peak levels of the flood events. However, it was observed that the model tends to underestimate the magnitude of the floods. This suggests that while the model was effective in simulating the general behavior and characteristics of the flood events, there is a room for future improvement for accurately reproducing the exact magnitude of the flooding.

Furthermore, composite analysis has been performed using ERA5 reanalysis dataset to understand the atmospheric precursors . The results revealed that despite the absence of strong ENSO signal, these flood events are associated with regional SST and atmospheric circulation that favours convergence of wind at low level and southward shift of the subtropical upper level jet stream which rise to divergence at upper level over eastern Africa. All of these are conducive to the generation of heavy precipitation amounts that are much higher than the climatological values.

The promising findings suggest that integrating the WRF-Hydro model into the regional and national operational centers would be a beneficial to enhance their flood monitoring and early warning systems. As part of our forthcoming project, we will focus on configuring and fine-tuning the coupled WRF-Hydro model. Additionally, we will conduct further sensitivity experiments by incorporating observed precipitation data.

Author Contributions: Conceptualization, A.S., G.T. and T.D.; methodology, A.S. and G.T.; software, A.S.; validation, A.S.; formal analysis, A.S and G.T; investigation, A.S. and G.T.; resources, T.D; data curation, B.H.; writing—original draft preparation, A.S.; writing—review and editing, G.T. and T.D.; visualization, A.S., G.T and Y.Y; supervision, G.T.; project administration, A.S.; funding acquisition, T.D. All authors have read and agreed to the published version of the manuscript.

Acknowledgments: We acknowledge the funding from the International Development Association (IDA) of the World Bank to the Accelerating Impacts of CGIAR Climate (AICCRA) project. GTD is currently affiliated with Environment and Climate Change Canada.

Conflicts of Interest: The authors declare no conflict of interest.

Preprints (www.preprints.org) | NOT PEER-REVIEWED | Posted: 4 May 2023 doi:10.20944/preprints202305.0168.v1

Appendix A.

Appendix A.1. Surface infiltration

I_{max} is the function of spatially varying precipitation inputs and soil properties. P_x is excess precipitation or through fall from canopy and is given by:

$$P_x = max(0, Q_{wat}.\Delta t) \tag{A1}$$

where Q_{wat} is the water input to the soil surface, and Δt is the model time step in hours ($\Delta t = \Delta t_1.86400$). Q_{wat} is calculated depending on the existence of a snow layer and it accounts for rainwater, melting water from the bottom of the snow pack, soil surface dew rate adjusted for frost.

The term D_{total} is the total soil moisture content that can potentially infiltrate, which depends on soil properties:

$$D_{total} = \sum_{k=1}^{N} \Delta Z_k.(SMCMAX - SMC_k) \tag{A2}$$

where ΔZ_k and SMC_k are the thickness and volumetric soil moisture content of the k-th soil layer (k = 1, ..., N = 4), respectively; and SMCMAX is the saturated volumetric soil moisture content dependent on soil type.

Appendix A.2. Model Performance Evaluation

$$NSE = \frac{\sum_{i=1}^{n}(O_i - \overline{O}) - \sum_{i=1}^{n}(P_i - O_i)^2}{sum_{i=1}^{n}(O_i - \overline{O})^2} \tag{A3}$$

$$RMSE = \sqrt{\frac{\sum_{i=1}^{n}(P_i - O_i)^2}{n}} \tag{A4}$$

$$RSR = \frac{RMSE}{STDEV_{obs}} = \frac{\sum_{i=1}^{n}(O_i - P_i)^2}{\sum_{i=1}^{n}(O_i - \overline{O})^2} \tag{A5}$$

Appendix A.3. Supplementary figures

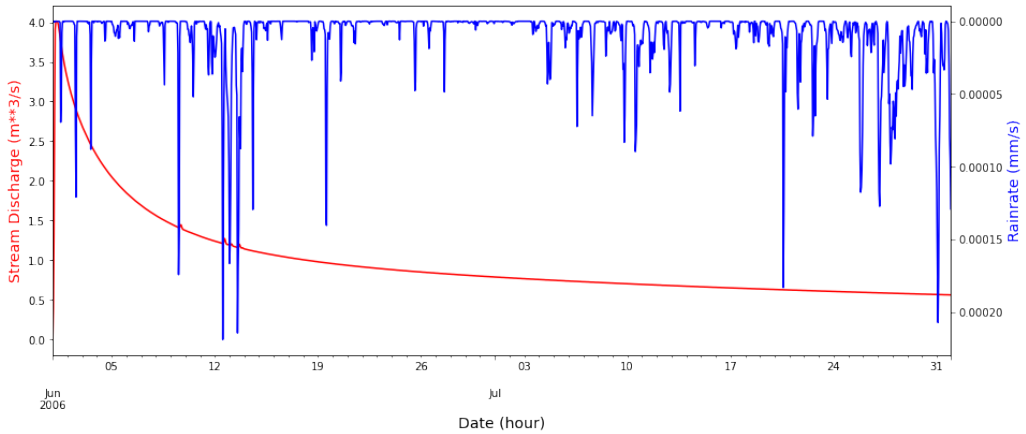

Figure A1. Stream Discharge with hourly time step at the outlet of Dechatu river (red), domain mean (D3) rain rate (blue) for a period of two months June 1 to July 31, 2006.

Preprints (www.preprints.org) | NOT PEER-REVIEWED | Posted: 4 May 2023 doi:10.20944/preprints202305.0168.v1

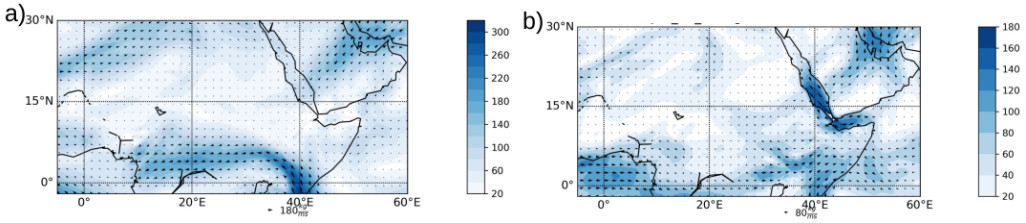

Figure A2. a) a) Integrated moisture flux [$kgm^{-1}s^{-1}$] for April [12-16] avg 2007, b) Integrated moisture flux [$kgm^{-1}s^{-1}$] anomaly for April [12-16] avg 2007 - [1991-2020].

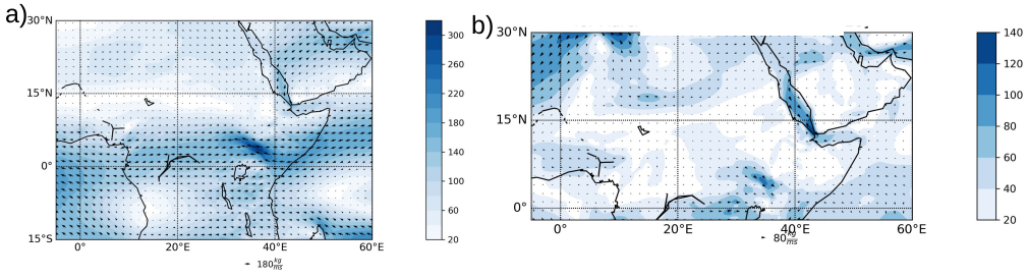

Figure A3. a) Integrated moisture flux [$kgm^{-1}s^{-1}$] for March [17-21] avg, 2005, b) Integrated moisture flux [$kgm^{-1}s^{-1}$] anomaly for March [17-21] avg, 2005 - [1991-2020].

References

1. Tramblay, Y.; Villarini, G.; Zhang, W. Observed changes in flood hazard in Africa. *Environmental Research Letters* **2020**, *15*, 1040b5.
2. Nations, U. World urbanization prospects: The 2001 revision. Data tables and highlights. *World Urban Prospect 2003 Revis* **2002**, pp. 1–195.
3. Alderman, K.; Turner, L.R.; Tong, S. Floods and human health: a systematic review. *Environment international* **2012**, *47*, 37–47.
4. Di Baldassarre, G.; Montanari, A.; Lins, H.; Koutsoyiannis, D.; Brandimarte, L.; Blöschl, G. Flood fatalities in Africa: from diagnosis to mitigation. *Geophysical Research Letters* **2010**, *37*.
5. Billi, P.; Alemu, Y.T.; Ciampalini, R. Increased frequency of flash floods in Dire Dawa, Ethiopia: Change in rainfall intensity or human impact. *Natural Hazards* **2015**, *76*, 1373–1394.
6. Erena, S.H.; Worku, H. Flood risk analysis: causes and landscape based mitigation strategies in Dire Dawa city, Ethiopia. *Geoenvironmental Disasters* **2018**, *5*, 16.
7. Erena, S.H.; Worku, H.; De Paola, F. Flood hazard mapping using FLO-2D and local management strategies of Dire Dawa city, Ethiopia. *Journal of Hydrology: Regional Studies* **2018**, *19*, 224–239.
8. Demessie, D.A. Assessment of flood risk in Dire Dawa town, eastern Ethiopia, using gis. PhD thesis, Addis Ababa University, 2007.
9. Douglas, I.; Alam, K.; Maghenda, M.; Mcdonnell, Y.; McLean, L.; Campbell, J. Unjust waters: climate change, flooding and the urban poor in Africa. *Environment and urbanization* **2008**, *20*, 187–205.
10. Olivier, J.G.; Van Aardenne, J.A.; Dentener, F.J.; Pagliari, V.; Ganzeveld, L.N.; Peters, J.A. Recent trends in global greenhouse gas emissions: regional trends 1970–2000 and spatial distributionof key sources in 2000. *Environmental Sciences* **2005**, *2*, 81–99.
11. Du, H.; Alexander, L.V.; Donat, M.G.; Lippmann, T.; Srivastava, A.; Salinger, J.; Kruger, A.; Choi, G.; He, H.S.; Fujibe, F.; et al. Precipitation from persistent extremes is increasing in most regions and globally. *Geophysical Research Letters* **2019**, *46*, 6041–6049.
12. Myhre, G.; Alterskjær, K.; Stjern, C. otros (2019). Frequency of extreme precipitation increases extensively with event rareness under global warming. *Scientific Reports*, *9*, 16063.
13. Coumou, D.; Robinson, A. Historic and future increase in the global land area affected by monthly heat extremes. *Environmental Research Letters* **2013**, *8*, 034018.
14. Zhang, X.; Alexander, L.; Hegerl, G.C.; Jones, P.; Tank, A.K.; Peterson, T.C.; Trewin, B.; Zwiers, F.W. Indices for monitoring changes in extremes based on daily temperature and precipitation data. *Wiley Interdisciplinary Reviews: Climate Change* **2011**, *2*, 851–870.
15. Camera, C.; Bruggeman, A.; Zittis, G.; Sofokleous, I.; Arnault, J. Simulation of extreme rainfall and streamflow events in small Mediterranean watersheds with a one-way-coupled atmospheric–hydrologic modelling system. *Natural Hazards and Earth System Sciences* **2020**, *20*, 2791–2810.
16. Lahmers, T.M.; Gupta, H.; Castro, C.L.; Gochis, D.J.; Yates, D.; Dugger, A.; Goodrich, D.; Hazenberg, P. Enhancing the structure of the WRF-hydro hydrologic model for semiarid environments. *Journal of Hydrometeorology* **2019**, *20*, 691–714.
17. Maidment, D.R. Conceptual framework for the national flood interoperability experiment. *JAWRA Journal of the American Water Resources Association* **2017**, *53*, 245–257.

18. Silver, M.; Karnieli, A.; Ginat, H.; Meiri, E.; Fredj, E. An innovative method for determining hydrological calibration parameters for the WRF-Hydro model in arid regions. *Environmental modelling & software* **2017**, *91*, 47–69.
19. Lahmers, T.; Castro, C.L.; Gupta, H.V.; Gochis, D.J.; ElSaadani, M. Optimization of precipitation and streamflow forecasts in the southwest Contiguous US for warm season convection. In Proceedings of the AGU Fall Meeting Abstracts, 2015, Vol. 2015, pp. H53A–1650.
20. Cerbelaud, A.; Lefèvre, J.; Genthon, P.; Menkes, C. Assessment of the WRF-Hydro uncoupled hydro-meteorological model on flashy watersheds of the Grande Terre tropical island of New Caledonia (South-West Pacific). *Journal of Hydrology: Regional Studies* **2022**, *40*, 101003.
21. Kerandi, N.; Arnault, J.; Laux, P.; Wagner, S.; Kitheka, J.; Kunstmann, H. Joint atmospheric-terrestrial water balances for East Africa: a WRF-Hydro case study for the upper Tana River basin. *Theoretical and Applied Climatology* **2018**, *131*, 1337–1355.
22. Diro, G.T.; Grimes, D.; Black, E. Large scale features affecting Ethiopian rainfall. In *African climate and climate change*; Springer, 2011; pp. 13–50.
23. Bekele-Biratu, E.; Thiaw, W.M.; Korecha, D. Sub-seasonal variability of the Belg rains in Ethiopia. *International Journal of Climatology* **2018**, *38*, 2940–2953.
24. Hersbach, H.; Dee, D. ERA5 reanalysis is in production. *ECMWF newsletter* **2016**, *147*.
25. Funk, C.; Peterson, P.; Landsfeld, M.; Pedreros, D.; Verdin, J.; Shukla, S.; Husak, G.; Rowland, J.; Harrison, L.; Hoell, A.; et al. The climate hazards infrared precipitation with stations—a new environmental record for monitoring extremes. *Scientific data* **2015**, *2*, 150066.
26. Schneider, U.; Becker, A.; Finger, P.; Meyer-Christoffer, A.; Ziese, M.; Rudolf, B. GPCC's new land surface precipitation climatology based on quality-controlled in situ data and its role in quantifying the global water cycle. *Theoretical and Applied Climatology* **2014**, *115*, 15–40.
27. Amatulli, G.; Domisch, S.; Tuanmu, M.N.; Parmentier, B.; Ranipeta, A.; Malczyk, J.; Jetz, W. A suite of global, cross-scale topographic variables for environmental and biodiversity modeling. *Scientific data* **2018**, *5*, 1–15.
28. Danielson, J.J.; Gesch, D. Global multi-resolution terrain elevation data 2010 (GMTED2010)(p. 26). US Department of the Interior. *US Geological Survey* **2011**.
29. Jarvis, A.; Reuter, H.; Nelson, A. E. Guevara (2008). Hole-filled seamless SRTM data V4, International Centre for Tropical Agriculture (CIAT).
30. Skamarock, W.C.; Klemp, J.B.; Dudhia, J.; Gill, D.O.; Liu, Z.; Berner, J.; Wang, W.; Powers, J.G.; Duda, M.G.; Barker, D.M.; et al. A description of the advanced research WRF model version 4. *National Center for Atmospheric Research: Boulder, CO, USA* **2019**, *145*, 145.
31. NCEP, F. operational model global tropospheric analyses, continuing from July 1999. *Research Data Archive at the National Center for Atmospheric Research, Computational and Information Systems Laboratory* **2000**, *10*, D6M043C6.
32. Gochis, D.; Yu, W.; Yates, D. The NCAR WRF-Hydro technical description and user's guide, version 3.0. *NCAR Technical Document* **2015**, *120*.
33. Schaake, J.C.; Koren, V.I.; Duan, Q.Y.; Mitchell, K.; Chen, F. Simple water balance model for estimating runoff at different spatial and temporal scales. *Journal of Geophysical Research: Atmospheres* **1996**, *101*, 7461–7475.
34. Chen, F.; Dudhia, J. Coupling an advanced land surface–hydrology model with the Penn State–NCAR MM5 modeling system. Part I: Model implementation and sensitivity. *Monthly weather review* **2001**, *129*, 569–585.
35. Moriasi, D.N.; Arnold, J.G.; Van Liew, M.W.; Bingner, R.L.; Harmel, R.D.; Veith, T.L. Model evaluation guidelines for systematic quantification of accuracy in watershed simulations. *Transactions of the ASABE* **2007**, *50*, 885–900.
36. Yucel, I.; Onen, A.; Yilmaz, K.; Gochis, D. Calibration and evaluation of a flood forecasting system: Utility of numerical weather prediction model, data assimilation and satellite-based rainfall. *Journal of Hydrology* **2015**, *523*, 49–66.
37. Jonkman, S.N. Global perspectives on loss of human life caused by floods. *Natural hazards* **2005**, *34*, 151–175.
38. Re, M. Natural catastrophes 2006: Analyses, assessments. *Positions. Munich Re Publications, Munich* **2007**.